# CARBON DIOXIDE ACTIVATION OF THE PLANE TREE SEEDS DERIVED BIO-CHAR
## Kinetic Properties and Application

by

***Vladimir M. DODEVSKI[a*], Bojan Ž. JANKOVIĆ[b], Miljana M. MIRKOVIĆ[a], Milan M. KRAGOVIĆ[a], Ivana M. RADOVIĆ[a], Filip M. VELJKOVIĆ[b], and Marija D. STOJMENOVIĆ[a]***

[a] Department of Materials Sciences, Vinca Institute of Nuclear Sciences, University of Belgrade, Belgrade, Serbia

[b] Department of Physical Chemistry, Vinca Institute of Nuclear Sciences, University of Belgrade, Belgrade, Serbia

Original scientific paper
https://doi.org/10.2298/TSCI190913064D

*Goal of this work is to establish technical feasibility and fundamentals of producing activated carbon from plane tree seeds biomass for porous materials derivation. Bio-chars produced via carbonization from plane tree seeds precursor were activated in $CO_2$ at 750 and 850 ºC, during various residence times. Their surface area and porosity were characterized by $N_2$ adsorption at 77 K. Surface areas of activated carbons can be correlated with kinetics mechanism and activation energy magnitudes of oxidation reaction by $CO_2$, which are closely related to applied activation temperature. Result showed that high temperature activated carbon had higher gas adsorption as compared to activated carbon obtained from lower temperature during two-hour residence time. Breakthrough behavior was detected at 850 °C where surface reactions dominate, and it is characterized by autocatalytic kinetic model under designed conditions. Both, temperature and $CO_2$ concentration in vicinity of solid surface effect on breakthrough time of adsorbent. Derived bio-chars are converted into high quality activated carbons, with surface area of 776.55 $m^2/g$, where micro-pores with pore diameters less than 2 nm prevail. Produced activated carbons have properties comparable with commercially available activated carbons, which can be successfully used for removal of harmful gaseous pollutants toward air purification.*

Key words: *plane tree seeds derived activated carbons, effectively $CO_2$ uptake, activation energy, micro-pores, surface area*

## Introduction

The urgent need for strategies to reduce global atmospheric concentrations of GHG has prompted action from national and international governments and industries, and a number of high-profile collaborative programs have been established including the Intergovernmental Panel on Climate Change and the Global Climate Change Initiative. Capture and sequestration of $CO_2$, predominant GHG, is the main strategy in these initiatives, as it offers the opportunity to meet increasing demands for fossil fuel energy in the short – to medium-term,

* Corresponding author, e-mail: vladimir@vin.bg.ac.rs

whilst reducing the associated GHG emissions in line with the global targets [1]. Carbon capture and storage (CCS) represents embody a group of technologies for capture of $CO_2$ from power plants, followed by compression, transport, and permanent storage. A critical point is that the deployment of CCS schemes is multi-faceted problem that requires shared vision and the world-wide collaborative efforts from governments, the policy makers and economists, as well as the scientists, engineers and venture capitalists. Bio-char synthesis usually consist of a carbonization step, while activated carbon synthesis can be performed by two well-known different ways, as physical and chemical activations, giving rise to the higher porous development. In last years, alternative synthesis procedures with aim of energy and/or chemical savings have been proposed. Thus, the non-conventional methods such as micro-wave heating [2, 3] and the hydrothermal carbonization treatment [4-6] are being analyzed for both, bio-chars and activated carbon preparations [7]. It is worth to mention, that porosity, surface chemistry and the yields of carbon-based adsorbents synthesized are the highly dependent on biomass composition, and the conditions used in the synthesis procedure.

The main objective of this study is to set a experimental design properties for adsorption of $CO_2$ onto biomass-derived bio-char by pyrolysis process of the plane tree seeds (PTS), using horizontal tubular reactor. The physical activation process of bio-char was performed. Namely, in the physical activation, the PTS precursor is initally carbonized and the resulting bio-char is submitted to controlled gasification with $CO_2$. Gasification step selectively removes many of reactive carbon atoms, generating the porosity and final activated carbon structure. When the $CO_2$ uses as gasifier agent, this reagent allows obtaining the activated carbon with wider porosity (which may even includes meso- and macro-pores), especially at the high burn-off values. One of the important goals of this work is kinetic analysis of gas adsorption process on obtained bio-chars. The relationship between kinetic parameters and established reaction mechanism was also discussed. The proposed kinetics of $CO_2$ adsorption on PTS derived bio-char was presented. The bio-based material was chosen in order to verify capabilities to give quality features endowed with large surface area and quality-developed porosity which would have potential to successfully reduce $CO_2$ emissions from polluted environments.

## Materials and methods

### *Bio-based material*

Material used in this research was harvested from the single trees of plane tree (*Platanus orientalis*) growing on plantation of Platan's trees outside the city (urban) environment. Diameter of PTS (*Platanus orientalis*) was about 1.5-2.5 cm. Achenes with their thin bristle fibers were used for the experimental work. Their length was up to about 1 cm and about 1 mm thick.

### *Carbonization (pyrolysis) process*

Raw PTS was peeled off and washed with water to remove any dirt and then dried at 80 ºC for 24 hours in an oven (Carbolite Gero GmbH & Co. KG, Germany) to reduce residual moisture content. Dried PTS was grounded (using planetary micro mill Pulverisette 7, Germany) and sieved, vibratory sieve shaker AS 200 basic (0.5-1.5 mesh), Retsch, Germany. Particle size fractions in a range of 0.5-1.5 mm were used for experiment.

About 20 g of material was placed in the furnace. During carbonization, purified nitrogen with gas flow rate of 500 $cm^3$ per min was used. Furnace temperature was increased from ambient temperature up to three operating temperatures as 650, 750, and 850 ºC, respec-

tively. When temperature reaches desired value, it was held for 1 hour. At the end of testing, gaseous flow of nitrogen in furnace was maintained during cooling until ambient temperature. The heating rate of furnace was amounted 4 °C per minute.

*Physical activation with $CO_2$*

Activation of samples was performed by $CO_2$. Activation of carbonized PTS sample was carried at two different operating temperatures as 750 ºC and 850 ºC for 0.3, 1, and 2 hours, under $CO_2$ gas flow (0.5 Lpm). About 5 g of obtained bio-char was loaded in the porcelain boat plate for every used activation temperature. Three different operating temperatures of 650, 750, and 850 ºC in programmed heating mode were used in additional tests for time duration needed for implementation of kinetic analysis, related to adsorption rates examination by $CO_2$. Considering activation, first, the nitrogen was allowed to flow through reactor and then followed by $CO_2$ gas. To maintain equal flow rate and pressure of both of the flaws, gas mixture was allowed to pass through mixing chamber. Flow of nitrogen was then stopped, and allowed only pure $CO_2$ gas to flow through reactor for adsorption measurements of the mass of $CO_2$ adsorbed per the mass of the adsorbent.

*Proximate/ultimate analysis and lignocellulosic composition*

Proximate and ultimate analysis procedure together with lignicellulosusic content determination for raw PTS material can be found elsewhere [8]

*The BET analysis and pore volume characteristics*

The isotherms based on adsorption/desorption of $N_2$ at 77 K were determined using a Sorptomatic 1990 Thermo Finnigan (Thermo Finnigan, today Thermo Fisher Scientific, Germany) device. Before measurements, the samples were degassed for 12 hours at 110 ºC and for 24 hours at 350 ºC under vacuum. The values of pore size distribution, meso-pore surface and micro-pore volume were calculated from obtained isotherms using the Software ADP Version 5.13 CE Instruments. Dollimore and Heal method was applied to obtain meso-pore size distribution, meso-pore volume ($V_{meso}$– DH) and meso-pore surface area ($S_{meso}$ – DH). The micropore volume ($V_{mic}$ – DR) was calculated according to the Dubinin-Radushkevich (DR) equation, while Dubinin's method modified by Kaganer was used to calculate the specific surface area of micro-pores. The pore size distribution as well as the mean pore size in micro-porous region and also micro-pore surface area ($S_{mic}$ – HK) was obtained by Horvath-Kowazoe method. Total specific surface area ($S_{tot}$) was estimated as sum of $S_{mic}$ – HK and $S_{meso}$ – DH.

## Theoretical backgrounds

For the purpose of determining the rate equation, it was assumed that term $\alpha$ represents the fraction of sites which are occupied by adsorbed gas or conversion fraction in a form:

$$\alpha = \frac{m(t) - m_o}{m_f - m_o} \tag{1}$$

where $m(t)$ is instantaneous mass of the solid during the exposure to $CO_2$. The parameters $m_o$ and $m_f$ are the initial and final mass of the sorbent, respectively. The differential kinetic equation can be expressed:

$$\frac{\mathrm{d}\alpha}{\mathrm{d}t} = k_{CO_2}(T) f_{CO_2}(\alpha) \tag{2}$$

where the temperature-dependent rate constant, $k_{CO_2}$ can be replaced with the Arrhenius equation:

$$\frac{\mathrm{d}\alpha}{\mathrm{d}t} = A_{CO_2} \exp\left(-\frac{E_{a,CO_2}}{RT}\right) f_{CO_2}(\alpha) \tag{3}$$

whereby $t$ is the time, $\mathrm{d}\alpha/\mathrm{d}t$ – the rate of monitored process, $A_{CO_2}$ – pre-exponential (frequency) factor that represents the gas molecules and solid adsorbent, $E_a$ – activation energy for adsorbing of gas molecules, R – universal gas constant (= 8.314 J/molK), $T$ – absolute temperature at which process takes place, while $f_{CO_2}(\alpha)$ represents function of adsorbing mechanism (kinetic model related to occurring of $CO_2$ adsorption process on carbonized material). Within isothermal experiments, Arrhenius equation is constant and rate of process is proportional to mechanism function. Therefore, when rate is plotted as a function of $\alpha$, its shape corresponds to mechanism function. Appropriate kinetics can be determined by evaluating nature of uptake rate data. This approach comprises the plot of $\ln(\mathrm{d}\alpha/\mathrm{d}t)$ *vs.* $\ln(1-\alpha)$. If either $\ln(\mathrm{d}\alpha/\mathrm{d}t)$ *vs.* $\ln(1-\alpha)$ are not linear, an $n^{\text{th}}$ ($n$ is reaction order) order reaction model is ordinarily considered. If curve is concave upward, reaction order $n$ would be greater than unity, and if curve is concave downward, $n$ would be less than unity.

The two functions, $Y(\alpha)$ and $Z(\alpha)$ can be introduced, where these functions allow determination of $f_{CO_2}(\alpha)$. The $Y(\alpha)$ and $Z(\alpha)$ functions can be obtained by transformation of the experimental data such as:

$$Y(\alpha) = \left(\frac{\mathrm{d}\alpha}{\mathrm{d}t}\right) \approx f_{CO_2}(\alpha) \tag{4}$$

$$Z(\alpha) = \left(\frac{\mathrm{d}\alpha}{\mathrm{d}t}\right) t = f_{CO_2}(\alpha) g_{CO_2}(\alpha) \tag{5}$$

It is convenient to normalize $Y(\alpha)$ plot within [0,1] interval. Shape of this plot (with maximum designated by $\alpha_M$) is characteristic for specific kinetic model and it can be used as diagnostic tool for determination of kinetic model. Maximum of $Z(\alpha)$ function (designated by $\alpha_p^{\infty}$) has characteristic values for kinetic models. Function $Z(\alpha)$ is useful for classification of possible kinetic model, $f_{CO_2}(\alpha)$ or $g_{CO_2}(\alpha)$, where $g_{CO_2}(\alpha)$ is integral form of $f_{CO_2}(\alpha)$. Function $Z(\alpha)$ is also normalized within [0,1] interval. By combination of the shape of function $Y(\alpha)$ with parameters $\alpha_M$, $\alpha_p$ ($\alpha$ value which corresponds to the peak of maximal rate) and $\alpha_p^{\infty}$, where $Z(\alpha)$ function has the maximum, the most suitable kinetic model may be estimated.

Avrami's fractional-order kinetic approach was recently developed and applied to describe adsorption of $CO_2$ on amine-functionalized adsorbents [9]. The general form of this model can be expressed:

$$\alpha(t) = 1 - \exp\left[-(kt)^m\right] \tag{6}$$

and in its logarithmic form as:

$$\ln\{-\ln[1-\alpha(t)]\} = m\ln(k) + m\ln t \tag{7}$$

where $\alpha(t)$ is time-dependent conversion fraction, $t$ – the time, $k$ – the overall rate constant, and $m$ represents the Avrami exponent. The Avrami exponent is a fractionary number, which reflects mechanism changes that may take place during the adsorption process [10].

Double logarithmic plot of $\ln\{-\ln[1-\alpha(t)]\}$ against $\ln t$ should give a straight line with slope which represents order $f$ reaction or Avramii exponent, $m$. If single process mechanism operates through monitored temperature range in a given extent of conversions, evaluated plots represent a set of parallel lines with a constant or approximately equal value of Avrami exponent, $m$. The corresponding values of $m$ for a range of established kinetic models were reported by Hancock *et al.* [11]. Rate constant $k$ is temperature-sensitive factor as $k = k_o\exp(-E_a/RT)$, where the $E_a$ is the single activation energy, while $k_o$ is a constant. Many gas-solid reactions take place in three stages, which may be described as follows: induction – formation of reaction sites or nuclei, acceleration – reaction interface increasing, and deceleration – reaction interface decaying. Selection of $g_{CO_2}(\alpha)$ function is based on shape of a reduced time plot which best describes experimental data. By calculating values of $\alpha$ for selected various kinetic equations and plotting them against $t/t_{0.50}$, where $t_{0.50}$ represents reaction's half-life (time value for 50% of $\alpha$). Theoretical predicted reacted fractions, $\alpha$, *vs.* $t/t_{0.50}$, for various reaction equations, against experimental data at all considered temperatures allows to make a selection of best model, which was adequate in description of adsorption. Data from a selected number of measurements should lie on single curve. This curve can be compared to that for any one of a number of different theoretical models.

## Results and discussion

### *Ultimate-proximate results and lignocellulosic content of selected precursor*

Table 1 shows the ultimate-proximate and lignocellulosic properties for raw bio-based material and activated material at 850 °C (2 hours).

**Table 1. Chemical compositions of PTS precursor and activated sample by $CO_2$ at 850 °C (2 hours)**

| Raw PTS | |
|---|---|
| Ultimate/proximate analysis* | |
| Moisture [%] | 9.43 |
| Ash [%] | 3.61 |
| Content of extractives in hot water [%] | 9.68 |
| Content of extractives in a mixture of toluene/ethanol [%] | 7.12 |
| Nitrogen [%] | 1.68 |
| Carbon [%] | 47.76 |
| Hydrogen [%] | 6.62 |
| Raw PTS – Lignocellulosic composition* | |
| Cellulose [%] | 33.79 |
| Hemicelluloses (the difference to 100%) [%] | 19.91 |
| Lignin [%] | 25.89 |
| HHV [kJ/kg] | 19817 |
| LHV [kJ/kg] | 18456 |
| Activated material at 850 °C [2 hours] | |
| Nitrogen [%] | 1.65 |
| Carbon [%] | 64.34 |
| Hydrogen [%] | 1.59 |
| HHV [kJ/kg] | 20966 |
| LHV [kJ/kg] | 20680 |

* Results are expressed in relation to absolute dry weight of the material.

Used raw material has acceptable heating values compared with wood and its products [12]. Also, raw PTS material contains the high content of the carbon, and the hydrogen, tab. 1.

On the other hand, the nitrogen content is low compared to C and H. Furthermore, the moisture content is significantly elevated than recommended value (3.0 wt.%), which means that the actual material in this condition is not suitable for long storage. The ash content is not so great, compared with palm of *Phoenix dactylifera* L. [13] or sugar cane [14]. Reduction in hydrogen upon activation, tab. 1, can certainly indicates on a reduced share of moisture. Upon activation process, thermal treatment at high temperatures will result in dehydration and devolatilization of precursor to gaseous product *i. e.* CO, while developing carbon-rich sample, C (%) = 64.34, *i. e.* activated carbon. Comparing literature data, HHV and LHV values obtained for activated material at 850 °C, tab. 1, are very close to values obtained for Macadamia nut shells (HHV = 20714 kJ/kg) and Cypress wood chips (LHV= = 18727 kJ/kg) which are rich in carbon, but these values are less than those identified for bituminous coal (HHV = 27061 kJ/kg and LHV = 24856 kJ/kg) [15]. The cellulose content, which is basic building blocks of the cell wall of plants, in raw material amounts 33.79%, tab. 1, which is pretty low value, probably, because it is a *fruit* of the plant. For plane tree (*Platanus orientalis* L.) Rowell [16] states that cellulose content amounts of 44%, without specifying that it is a date for *fruit* of the plant. In contrast, total lignin content of 25.89%, tab. 1, is slightly higher than for Klason's lignin content which amounts 21% in the case of plane tree. The content values of the extractives dissolved by hot water and in a mixture of toluene/ethanol are fairly high, probably because used material originates from physiologically active parts of the plant.

### *Sorption analysis*

Porosity analysis for all considered samples are presented in tab. 2.

**Table 2. Textural characteristics of activated carbons using the various calculations methods**

| Method | Conditions | Monolayer volume [$cm^3g^{-1}$] | Monolayer amount [$mmolg^{-1}$] | Surface area [$m^2g^{-1}$] | Micro-pore volume [$cm^3g^{-1}$] | Median pore diameter [nm] | Maximum pore diameter [nm] | Cumulative pore volume [$cm^3g^{-1}$] | Cumulative pore area [$m^2g^{-1}$] |
|---|---|---|---|---|---|---|---|---|---|
| Surface Area (BET) 2-parameters line | 2h: 750 | 98.01 | 4.3728 | 426.60 | – | – | – | – | – |
| | 0.3h:850 | 122.19 | 5.4518 | 531.87 | – | – | – | – | – |
| | 1h:850 | 165.74 | 7.3944 | 721.39 | – | – | – | – | – |
| | 2h:850 | 112.83 | 5.0341 | 491.12 | – | – | – | – | – |
| Mesopores - Barrett-Joyner-Halenda (BJH) | 2h: 750 | – | – | – | – | 6.8481 | 1.9264 | 0.0869 | 61.851 |
| | 0.3h:850 | – | – | – | – | 15.604 | 3.9470 | 0.1876 | 85.059 |
| | 1h:850 | – | – | – | – | 4.8389 | 3.6766 | 0.1603 | 129.350 |
| | 2h:850 | – | – | – | – | 8.4460 | 3.5385 | 0.1917 | 120.500 |
| Mesopores (Dollimore and Heal) | 2h: 750 | – | – | – | – | 4.4958 | 2.0298 | 0.0547 | 47.739 |
| | 0.3h:850 | – | – | – | – | 5.0446 | 1.9792 | 0.0738 | 62.645 |
| | 1h:850 | – | – | – | – | 5.0013 | 1.9967 | 0.1176 | 103.980 |
| | 2h:850 | – | – | – | – | 4.5437 | 1.9604 | 0.1008 | 94.306 |
| Micro-pores (Horvath-Kawazoe) | 2h: 750 | – | – | – | – | 0.5630 | 0.5247 | 0.1706 | 525.920 |
| | 0.3h:850 | – | – | – | – | 0.5376 | 0.5139 | 0.2123 | 684.020 |
| | 1h:850 | – | – | – | – | 0.5416 | 0.5036 | 0.2886 | 923.680 |
| | 2h:850 | – | – | – | – | 0.5591 | 0.5217 | 0.1994 | 609.680 |
| Micro-pores (Dubinin-Raduskevich) | 2h: 750 | 109.37 | 4.8795 | 476.00* | 0.1690 | – | – | – | – |
| | 0.3h:850 | 131.55 | 5.8692 | 572.59* | 0.2033 | – | – | – | – |
| | 1h:850 | 178.41 | 7.9598 | 776.55* | 0.2757 | – | – | – | – |
| | 2h:850 | 123.44 | 5.5072 | 537.27* | 0.1908 | | | | |

* Modified by the Kaganer.

Greatest surface area and availability in monolayer were obtained for the sample activated at 850 °C for 1 hours. Including BJH analysis for meso-pores, maximum and median pore diameters have been achieved in shortest residence time at highest temperature, but cumulative pore area is the most common at 850 °C for 1 hours. Dollimore and Heal approach gives more variability in results of maximum and median pore diameters, but still the cumulative pore area is the highest at 850 °C for 1 hours.

Latter value is lower than that obtained by BJH approach. If we consider the results related to characteristics of micropores, the highest value of all listed magnitudes are obtained mainly for sample activated at 850 °C for 1 hours, but also results obtained for sample activated at 850 °C for 2 hours can also come to the fore.

Based on obtained results, we can conclude that material is characterized by high surface area and well-developed pore structure, especially with high micropore volumes. So, obtained material shows high capabilities for efficient $CO_2$ uptake performance, which arises due to pore's size distribution of carbons being shifted towards small micropores, and even for samples with high surface area.

The melting and fusion process of lignin and other small organic molecules can lead to the smooth surface formation. From these results, it is obvious that the porosity is more developed at the higher temperatures, where such open pores with the dominant micropores are the main sources of the high surface area. Gas capture capacity is in accordance with availability of narrow pore size distribution in activated carbon (850 °C 2 hours), and this is important factor influenced on both, textural and surface chemistry properties on their capture performances.

### *Kinetic analysis and mechanism*

Figures 1(a) and 1(b) shows conversion curves as well as corresponded rate curves of $CO_2$ gas adsorption at solid carbonized material where the process is monitored at three various temperatures $T$ = 650, 750, and 850 °C, during two hours of exposing. Curves at 650 °C and 750 °C exhibit deceleratory shape during entire time interval. However, at very beginning of the process, $\alpha - t$ curve at 850 °C shows a certain incubation period, and subsequently manifests deceleratory behavior.

If the rate curve has a maximum at $\alpha = 0$ or $t = 0$, then the reaction-order mechanism can takes place. If the rate curve exhibits a clearly straight linear behavior then we have a first-

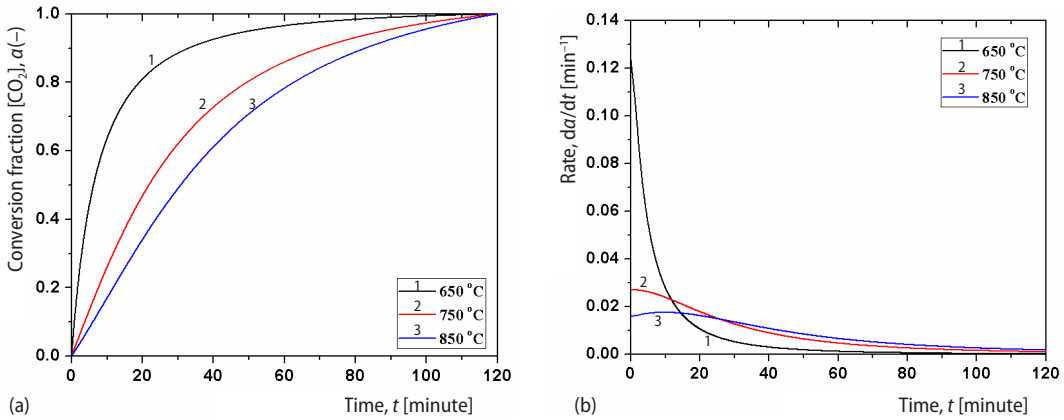


**Figure 1. (a) The $\alpha - t$ curves and (b) the rate curves of $CO_2$ adsorption process onto solid bio-char, monitored at various temperatures (650, 750, and 850 °C), during exposing of two hours**

order reaction process. The concave and convex shape curve requires a more complicated reaction model. If the curve is concave upward, the reaction model could be either $n^{th}$ order reaction with $n > 1$ or a multi-exponential decay having anywhere from two to a continuous distribution of the rate constants. Following case is one which includes the fact when the process rate does not achieve maximum at $\alpha = 0$ or $t = 0$, and the rate rises due to the intrinsic chemical kinetics. When initial reaction rate is zero at $t = 0$, the autocatalytic model such as a nucleation reaction model can be used to characterize the rate curve [17].

On the other hand, the initial rise could be due to the transport through a porous material from either heat transfer or the mass transfer through particle [18]. Based on the shape of rate curves, it can be assumed that adsorption process at temperatures of 650 °C and 750 °C may be follows $n^{th}$ order mechanisms, while the adsorption process at 850 °C should be monitored by the accelerator (probably autocatalytic) mechanism. Figure 2 shows the normalized $Y(\alpha)$ and $Z(\alpha)$ functions at the various temperatures ($T$ = = 650, 750, and 850 °C).

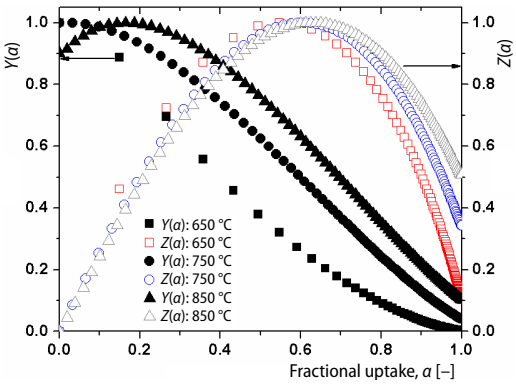


**Figure 2. The $Y(\alpha)$ and $Z(\alpha)$ functions for $CO_2$ adsorption process onto solid bio-char, at temperatures of 650, 750 and 850 °C**

It can be observed that $Y(\alpha)$ functions vary with temperature, while varying of $Z(\alpha)$ functions is much less at lower values of $\alpha$, and is a much more pronounced at higher $\alpha$ ($\alpha > 60\%$). Only for 850 °C, the $Y(\alpha)$ function shows visible maximum, while maximums of $Y(\alpha)$ functions at other temperatures stand at zero values. This behavior of $Y(\alpha)$ maxima indicates on presumably changing of reaction mechanism.

**Table 3. Values of $\alpha_M$, $\alpha_p^\infty$, and $\alpha_p$ at the different temperatures (650, 750, and 850 °C)**

| $T$ [°C] | $\alpha_M$ | $\alpha_p^\infty$ | $\alpha_p$ |
|---|---|---|---|
| 650 | 0 | 0.547 ± 0.002 | 0 |
| 750 | 0 | 0.609 ± 0.003 | 0 |
| 850 | 0.165 ± 0.002 | 0.638 ± 0.003 | 0.165 ± 0.002 |

Table 3 shows characteristic parameters values ($\alpha_M$ and $\alpha_p^\infty$) attached to maxima of $Y(\alpha)$ and $Z(\alpha)$ functions as well as the peak position values ($\alpha_p$) at rate curves.

Based on determined $\alpha_M$, $\alpha_p^\infty$, and $\alpha_p$ values, tab. 3, $n^{th}$ order (with $n \neq 1$) reaction model can be expected at a temperatures of 650 °C to 750 °C, while at highest temperature of 850 °C, the some of semi-empirical kinetic models should be taken into account [19].

Figure 3 a shows comparison of experimental and theoretical reduced-time plots in order to assesses best kinetic model that describes the actual process at various temperatures.

Theoretical reduced-time plots were designed for following groups of kinetic models as: phase-boundary models, contracting cylinder (R2) and contracting sphere (R3); first-order (Mample) model (F1); Avrami-Erofeev kinetic models, A1.5 ($m$ = 1.5), A2 ($m$ = 2.0), A3 ($m$ = 3.0) and A4 ($m$ = 4.0); and diffusion models, 1-D diffusion (−D1), 2-D diffusion (−D2), and 3-D diffusions, −D3 (Jander) and −D4 (Ginstling-Brounshtein).

From fig. 3(a), it can be observed that experimental points follow the *mixture* of several kinetic models, with varying the temperature. At 650 °C, for $\alpha < 0.55$, the experimental points follows reduced-time plot for F1 model, while for $\alpha > 0.55$, the points follow the 2-D diffusion (−D2) model. At the temperature of 750 °C, the experimental points follow the first-

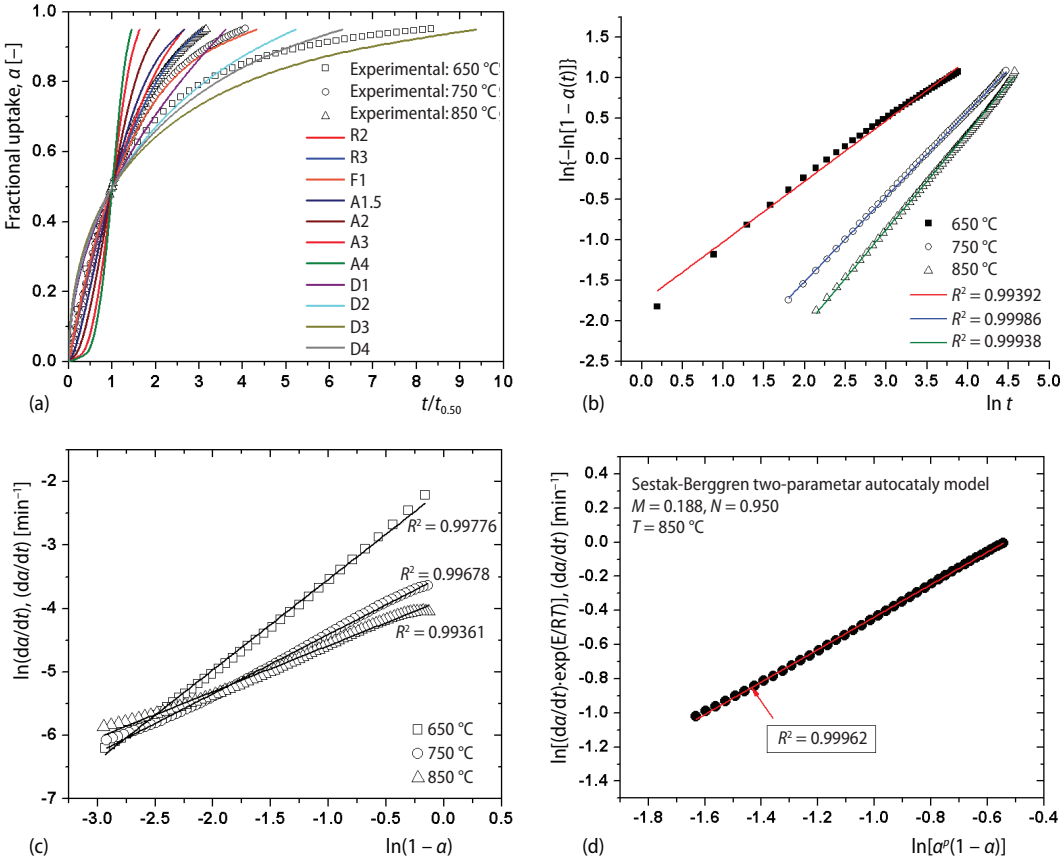


**Figure 3. (a) Comparison of experimental and theoretical reduced-time plots, (b) the *ln-ln* plots obtained from Avrami method, (c) dependence of ln(d$\alpha$/d$t$) against ln(1 – $\alpha$) profiles, and (d) Šesták-Berggren SB($M$, $N$) plot for 850 °C, with designated values of kinetic exponents**

order (Mample) model (F1). Finally, at 850 °C, the experimental points follow the reduced-time plot for phase-boundary model, R3 (the contracting sphere). These results indicate that there is a drastic change in rate-determining step. In order to clarify the precise reaction kinetic mechanism for $CO_2$ adsorption, the Avrami's double logarithmic (*ln-ln*) plots method was applied.

Figure 3(b) shows linear *ln-ln* plots obtained from Avrami method, in order to estimate Avrami exponent, $m$, and overall rate constant $k$, at every considered temperature. Table 4

**Table 4. Avrami's fractional order kinetic model parameters (ln($k$), $k$ and $m$), as well as the values of the kinetic parameters (ln($k$), $k$ and $n$) obtained from linear correlation of ln(d$\alpha$/d$t$) against ln(1 – $\alpha$)**

| $T$ [°C] | Avrami's fractional order kinetic model | | | | ln(d$\alpha$/d$t$) *vs.* ln(1 – $\alpha$) plots | | |
|---|---|---|---|---|---|---|---|
| | $\Delta\alpha$ | ln[$k$] | $k$ [min$^{-1}$] | $m$ | ln[$k$] | $k$ [min$^{-1}$] | $n^*$ |
| 650 | 0.15-0.95 | –2.36223 | 0.09421 | 0.749 ± 0.009 | –2.11212 | 0.12098 | 1.426 ± 0.011 |
| 750 | 0.16-0.95 | –3.44234 | 0.03199 | 1.046 ± 0.001 | –3.47308 | 0.03102 | 0.934 ± 0.007 |
| 850 | 0.14-0.95 | –3.72560 | 0.02410 | 1.199 ± 0.003 | –3.86055 | 0.02106 | 0.724 ± 0.007 |
| Average | – | –3.17672 | 0.05010 | 0.998 ± 0.004 | –3.14858 | 0.05769 | 1.028 ± 0.008 |

* Reaction order.

lists the values of ln($k$), $k$ and $m$ calculated from intercepts and slopes of obtained straight lines at various temperatures.

Based on calculated Avrami's exponent ($m$), tab. 4, the value of $m$ = 0.749 at 650 °C corresponds to medium value between two reaction models such as the first-order reaction (F1) ($m$ = 1.000) and 2-D (−D2) diffusion reaction ($m$ = 0.570) [11]. Value of $m$ (= 1.046) obtained at 750 °C corresponds approximately to first-order reaction model. At highest temperature (850 °C), $m$ = 1.199 lies between the values of $m$ which can be attributed to R2 and R3 models [11].

Therefore, there is a drastic change in reaction mechanism with a change in temperature, so that process cannot be described through single-step kinetic model. According to Avrami theory, when number of nuclei is constant and domains grow with diffusion-controlled velocity, $m$ takes value which was presented in tab. 4 at 650 °C. Avrami's exponent at temperatures of 750 °C and 850 °C has a value between 1 and 1.5, where this indicates that crystallization could start from surface, and where the values of $m$ = 1.046 and 1.199 indicate 1-D growth of nuclei with decreasing adsorption rate. Thus, although initial formation of adsorption sites may be homogeneous on uniformly exposed surface, additional adsorption may be formed preferentially in neighborhood of existing adsorption sites, leading to deviation from homogeneous formation of adsorption sites and Avrami exponent becomes larger than unity [19]. A difference in value of Avrami's exponent, which also describes how fast adsorption process occurs, suggests a difference in the adsorption mechanism.

In addition, the dependence of ln(d$\alpha$/d$t$) against ln(1 – $\alpha$), fig. 3(c), shows a high linear correlations of established plots at all temperatures, where kinetic parameters are shown in tab. 4. It can be observed that with an increasing of temperature, the reaction-order value decreases. Fractional reaction order may indicate that reaction is topochemical and limited by diffusion. Namely, the fractal parameters may be measure of heterogeneity at reaction interface and would facilitate the manipulation of interface reaction in desired directions [20]. Taking the values of ln($k$), which are calculated on the basis of both approaches, Arrhenius dependencies of ln($k$) = = ln$A$ – $E_a$/R$T$ were estimated. With such dependence, the following values of the pre-exponential factor ($A$) and the apparent activation energy ($E_a$) were calculated: $A = 3.575 \cdot 10^{-5}$ min$^{-1}$, $E_a$ = –59.7 ± 2.0 kJ/mol (Avrami's approach), and $A = 5.043 \cdot 10^{-6}$ min$^{-1}$, $E_a$ = –76.5 ± 2.3 kJ/mol (reaction-order approach), respectively. The $A$ values show low factors which often indicate the surface reaction. Such low magnitude of pre-exponential factor can indicates on *tight* complex formed during process. It should be noted that negative value of $E_a$ may suggests that rise in temperature did not favor $CO_2$ adsorption onto bio-chars. This may depends largely on the ratio of $E_a$, which can be attributed to activation energy needed for adsorption to an external surface of adsorbent, and activation energy for adsorption into pores ($E_p^*$). The term $E_p^*$ can be calculated from intra-particle diffusion coefficient $D$ [m$^2$s$^{-1}$] values estimated for every temperature. Namely, intra-particle diffusion coefficient can be determined using main equations related to Fick's law [21]. Thereafter, the value of $E_p^*$ may be obtained from equation $D = D_0\exp(-E_p^*/\mathrm{R}T)$ and then from $\ln(D) = \ln(D_0) - E_p^*/\mathrm{R}T$ [22]. The following values of intra-particle diffusion coefficient ($D$) were obtained: $4.847 \cdot 10^{-9}$ m$^2$/s (650 °C), $2.851 \cdot 10^{-9}$ m$^2$/s (750 °C), and $2.502 \cdot 10^{-9}$ m$^2$/s (850 °C), respectively. In addition, after these calculations, the following value of $E_p^*$ was obtained: $E_p^*$ = –29.0 ± 1.0 kJ/mol. The negative $E_a$ value indicates exothermic reaction and low value suggests that adsorption process of $CO_2$ onto solid surface might be by the physical adsorption. It means that rate-limiting step of $CO_2$ adsorption onto bio-char involves predominantly the physical process. On the other hand, it was found that $E_p^*$ (–29.0 kJ/mol) > $E_a$ (–76.5 kJ/mol), but both terms are still negative, and this means that $CO_2$

molecules are much faster moves, and the lower energy is needed for them to diffuse into solids. Moreover, this behavior is correlated well with calculated values of $D$, which decrease with an increasing of temperature.

Lowest value of $D$ is observed at 850 °C, where we can expect the change in behavior of some kinetic parameters. Namely, the rate constant ($k$) decreased with an increasing temperature, and it is disadvantage for $CO_2$ adsorption at high temperature, taking into account exothermic nature of the process. It is obvious that sudden change in adsorption exists at highest temperature. Considering that $E_p^* > E_a$ and $D$ values, we can conclude that rate-limiting step of $CO_2$ adsorption is probably governed by diffusion controlled process, especially at temperatures below 850 °C.

The mentioned diffusion reaction scheme corresponds to fractional reaction order values, and usually for $n$-fractal numbers within $n > 1$ [23]. This can be checked *via* correlation that links the position of $Z(\alpha)$ maximum ($\alpha_p^\infty$) and reaction order value:

$$\alpha_p^\infty = 1 - n^{\frac{1}{(1-n)}}. \tag{8}$$

Based on the established values of $\alpha_p^\infty$, tab. 3, by iterative calculation procedure, the following values of reaction-orders ($n$) were obtained: $n$ = 1.568 650 °C ($n > 1$), $n$ = 1.133 750 °C ($n > 1$), and $n$ = 0.968 850 °C ($n < 1$), respectively.

The parameter $n$ of fractional order may reflect effect of driving force which was related to adsorption apparatus and filling mode of adsorbent. From obtained results, we can see that parameter $n$ suffer great change with an increasing of temperature. It can be observed that $n$ reaches maximum at 650 °C, indicating large driving force at that temperature. This large driving force promotes facilitated $CO_2$ diffusion into adsorbent. At highest temperature this force is very weakened, which can be seen from decline in $n$ parameter value below unity. Values of $n$ for 650 °C and 750 °C, together with Arrhenius parameters ($A = 5.043 \cdot 10^{-6}$ min$^{-1}$, $E_a$ = = –76.5 kJ/mol) were used for modeling of adsorption rate curves (through general rate-law equation such as: $d\alpha/dt = A\exp(-E_a/RT)(1-\alpha)^n$). Figure 4 shows comparison between experimentally obtained and simulated rate curves for $CO_2$ adsorption process onto PTS derived bio-char at temperatures of 650 °C and 750 °C.

It can be observed that a very good agreement between experimental and simulated rate curves exists, so that fractal reaction model very well describes the adsorption process at 650 °C and 750 °C. On the other hand, it was found that process which take place at 850 °C can be best described with truncated Šesták-Berggren SB($M$,$N$) two-parameter autocatalytic reaction model. Namely, from tab. 3, we have $0 < \alpha_M < \alpha_p^\infty$ and $\alpha_p^\infty \neq 0.632$ at 850 °C, which strongly indicates that truncated SB($M$,$N$) model was suitable. General differential model equation of truncated SB($M$,$N$) model can be expressed as $f(\alpha) = \alpha^M(1-\alpha)^N$. For adsorption process, parameter $M$ reflects how fast adsorption process is, and also indicates a more important role

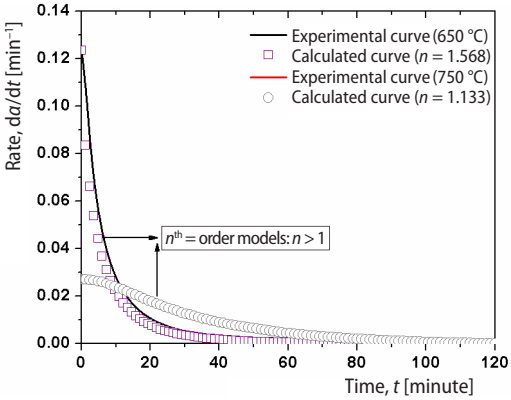


**Figure 4. Comparison between experimentally obtained and simulated rate curves for $CO_2$ adsorption process onto PTS derived bio-char at 650 °C and 750 °C**

of adsorbed gas on solid surface, while parameter $N$ reflects level of *chemical* complexity. It also appears that higher value of second SB exponent ($N > 1$) indicates increasing reaction complexity. According to SB($M$,$N$) model and eq. (2), the eq. (3) can be transformed through logarithmic operations:

$$\ln\left[\left(\frac{\mathrm{d}\alpha}{\mathrm{d}t}\right)\exp\left(\frac{E_a}{\mathrm{R}T}\right)\right] = \ln A + N\ln\left[\alpha^p\left(1-\alpha\right)\right] \tag{9}$$

where $M$ and $N$ are reaction orders. The ration of $M$ to $N$ is designated by the $p$ and equals to the $\alpha_M/(1-\alpha_M)$.

Kinetic exponent $N$ can be derived from slope of $\ln[(\mathrm{d}\alpha/\mathrm{d}t)\exp(E_a/\mathrm{R}T)]$ against $\ln[\alpha^p(1-\alpha)]$ for $\alpha \in [0.20,0.80]$, and intercept is $\ln A$. Second exponent $M$ may be calculated from $M = pN$. For observed temperature of 850 °C, the SB($M$,$N$) plot was evaluated and actual plot is shown in fig. 3(d). From estimated SB plot, the following values of SB kinetic exponents were obtained: $M = 0.188$ and $N = 0.950 \pm 0.003$ ($p = 0.198$). However, the high SB linear correlation at 850 °C was obtained for following pair of Arrhenius parameters as: $E_a = 37.7 \pm 1.1$ kJ/mol, and $A = 1.669 \cdot 10^0$ min$^{-1}$. If we compare this result with a results obtained for other two temperatures (650 °C and 750 °C), we can see that we have the positive activation energy and much higher magnitude of pre-exponential factor. It should be noted that calculated value of $E_a$ corresponds to later stage of the process at elevated temperature, where *switch off* takes place in previous mechanism (to a temperature of 850 °C). Low value of $M$ exponent (0.188) indicates on adsorption slowdown. Adsorption process at 850 °C became slower, according to decreased value of $M$. In actual case, concentration of $CO_2$ is dropping down, and just on this temperature the breakthrough occurs [24].

The breakthrough obviously depends on residence time of $CO_2$ in vicinity of reaction surface. On the other hand, positive value of $E_a = 37.7$ kJ/mol can be interpreted from equation: $E_a = E_s - \Delta H_{\mathrm{ads}}^{\mathrm{CO_2}} \cong -\Delta H_{\mathrm{ads}}^{\mathrm{CO_2}}$ (where $E_a$ is activation energy, $E_s$ – the activation energy for surface reaction, and $\Delta H_{\mathrm{ads}}^{\mathrm{CO_2}}$ – the enthalpy of $CO_2$ adsorption), where $E_a$ is a positive number. However, situation may arises in which negative $E_a$ value is observed, as in previous cases at 650 °C and 750 °C, and that is, the reaction rate decreases with an increasing of temperature. Since the enthalpy of adsorption is almost always negative, activation energy can be either positive or negative, depending on magnitudes of $E_s$ and $\Delta H_{\mathrm{ads}}^{\mathrm{CO_2}}$. In the actual case, we can assume that in adsorption process, the surface reactions are dominated (the internal diffusion is lost) and actually, the surface reaction is usually rate-limiting. In this case, the $E_s$ cancels $\Delta H_{\mathrm{ads}}^{\mathrm{CO_2}}$ transforming aforementioned relation into correlation $E_a = E_s + \Delta H_{\mathrm{ads}}^{\mathrm{CO_2}}$ (endothermic effects) and this behavior is typical for multi-step mechanism of surface catalyzed reactions [25]. It is turning point in sign behavior of activation energy ($E_a$), which explains its positive value at 850 °C. Figure 5 shows comparison between experimentally obtained and simulated (using the SB model) rate curves at 850 °C.

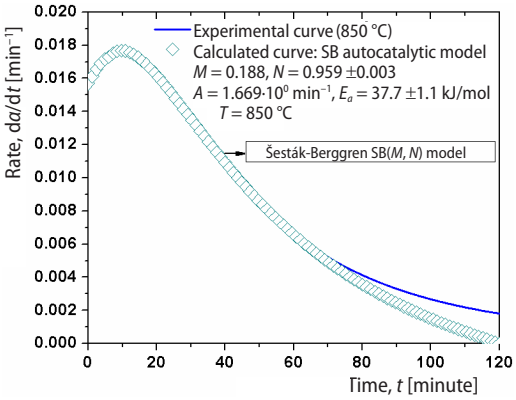


**Figure 5. Comparison between experimentally obtained and simulated, SB (*M* , *N*) model, rate curves at 850 °C**

It can be observed that the SB($M$, $N$) autocatalytic model very well describes ad-

sorption process of $CO_2$ monitored at 850 °C. Certain deviations still exist at higher $t$ values ($t > 80$ min), where actual model represents a kind of accommodation function (which compensates distortion from ideal process), which includes kinetic parameters that can be viewed as apparent under studied conditions, such as: type of precursor, particle size, type of reactor, the $CO_2$ gas flow, operating temperature, *etc.*

### *Application of PTS activated carbons*

Table 5 shows comparison of characteristics of wood and grass biomasses together with surface area and porosity of activated carbons derived from them, with the same quantities related to PTS activated carbon obtained in this work.

By comparing results in tab. 5, it can be seen (since PTS represents *fruit* of *Platanus orientalis* which was hardwood) that surface area and porosity of PTS activated carbon are very close to those related to HW. However, BET surface area is higher than for yellow poplar, redwood and switchgrass, tab. 5. Micro-pore volume of PTS activated carbon is very similar with ones attached to HW, but meso-pore volume is slightly higher for PTS, than previously mentioned.

**Table 5. Comparison of various characteristics and surface/porosity features of wood and grass biomasses related to end-product, the activated carbon, with those related to PTS in this work**

| Materials | Properties | Hardwood* | | | Softwood* | | Grass* | PTS*** |
|---|---|---|---|---|---|---|---|---|
| | | HW*,** | CO*,** | YP*,** | RW*,** | WP*,** | SG*,** | This study |
| Raw material | Ash [%] | 0.54 | 1.76 | 1.26 | 0.17 | 0.57 | 1.80 | 3.61 |
| | Carbon [%] | 44.82 | 47.79 | 47.67 | 25.99 | 49.30 | 43.22 | 47.76 |
| | Hydrogen [%] | 6.06 | 5.82 | 6.33 | 7.71 | 6.48 | 5.22 | 6.62 |
| Activated carbon | BET surface area [$m^2g^{-1}$] | 730 | 915 | 686 | 625 | 1050 | 612 | 721.4 |
| | Micro-pore volume (< 2 nm) [$cm^3g^{-1}$] | 0.27 | 0.28 | 0.25 | 0.24 | 0.33 | 0.22 | 0.29 |
| | Meso-pore volume (2-50 nm) [$cm^3g^{-1}$] | 0.10 | 0.85 | 0.25 | 0.07 | 1.06 | 0.18 | 0.19 |

* [26]
** HW – mixed hardwood, CO – chestnut oak, YP – yellow poplar, RW – redwood, WP – white pine, SG – switchgrass
*** High gas uptake (adsorption capacity) equals to 7.96 mmol/g, tab. 2

Certain differences in results shown in tab. 5 arise from the fact that starting bio-chars have different properties and differ in reaction kinetics ($C_{(s)} + CO_{2(gas)} \rightarrow 2CO_{(gas)}$, as *gasification* that develops porosity by removing carbon atoms), as well as in procedures for obtaining the activated carbon, afterwards. Ratio of cellulose, hemicelluloses and lignin in charred precursor determine properties of activated carbon, but in different ways and in proportion to their initial mass content – thermally labile cellulose and hemicelluloses contribute to pore system, while more resistant lignin is retrieved in solid carbon matrix. Recently, it was reported [27] that porosity is generated during activation process by selective oxidation of weakest, un-structured regions in charred material, where fine pores are developed. Kinetics of oxidation process seems to be a key factor in controlling porosity. This fact was explained previously. Taking into account results obtained, it can be concluded that PTS activated carbon (has the moderate BET surface area, 721.4 $m^2/g$, tab. 2, which contains large proportion of micropores (< 2 nm); PTS bio-char has faster oxidation reaction in $CO_2$, supported by higher kinetic parameters at temperature of 850 °C) is desirable for gas phase applications based on adsorption in molecular-sized micropores, such as gas cleaning, storage, and separation. It should be noted that at

high temperatures, as applied in this study (850 °C), some bio-chars may still contain small amounts of aliphatic carbon from un-transformed cellulose, but major content is lignin carbon with fused aromatic rings. So, lignin-derived carbon provides matrix for development of micro-porosity. From these facts it follow that porosity is generated in reaction of $CO_2$ with organized aromatic structures of lignin-derived carbon, which exists at high temperatures in carbonization process. However, if disordered hemicelluloses-derived carbon structures were still present in bio-char at high temperatures, they would be oxidized by carbon dioxide, but would not contribute much to development of porosity and increase in surface area.

## Conclusion

This study demonstrates that charred carbon by-products produced during carbonization (pyrolysis) of PTS biomass can be successfully converted into porous (activated) carbons. After carbonization performed at various operating temperatures (650, 750, and 850 °C), the activated carbons were prepared from bio-chars through physical activation by $CO_2$. The micro--pore and meso-pore textures were carried out using $N_2$ adsorption at 77 K. The obtained activated carbons are predominantly micro-porous, where the highest surface area was established for activated carbon produced at 850 °C with one hour residence time. It was observed that activation temperature has a strong influence on developing of porous structure and opening on the surface of activated carbon. Breakthrough behavior was detected at operating temperature of 850 °C, where surface reactions dominate. Obtained activated carbons derived from PTS bio-chars are comparable with commercial activated carbons suitable for adsorption in molecular-sized micro-pores, such as gas cleaning, storage, and separations. Present carbons are first examples of plane tree seeds derived porous materials adapted for high gases uptake performances, where products obtained, satisfy requirements for both, low pressure (presence of micro-pores smaller than 2 nm) and high pressure (the high surface area, 776.55 $m^2g^{-1}$) $CO_2$ uptake.

## Acknowledgment

This research work was partially supported by the Serbian Ministry of Education, Science and Technological Development under the projects numbered as 172015, III45005, TR34011, TR34013, 172018 and III45012.

## References

[1] Jacobson, M. Z., Review of Solutions to Global Warming, Air Pollution, and Energy Security, *Energy & Environmental Science*, *2* (2009), pp. 148-173
[2] Ao, W., *et al*., Microwave Assisted Preparation of Activated Carbon from Biomass: A Review, *Renewable and Sustainable Energy Reviews, 92* (2018), Sept., pp. 958-979
[3] Ahmed, M. J., Application of Agricultural Based Activated Carbons by Microwave and Conventional Activations for Basic Dye Adsorption: Review, *Journal of Environmental Chemical Engineering, 4* (2016), 1, pp. 89-99
[4] Hu, B., *et al*., Engineering Carbon Materials from the Hydrothermal Carbonization Process Of Biomass, *Advanced Materials, 22* (2010), 7, pp. 813-828
[5] Huff, M. D., *et al*., Comparative Analysis of Pinewood, Peanut Shell, and Bamboo Biomass Derived Biochars Produced Via Hydrothermal Conversion and Pyrolysis, *Journal of Environmental Management, 146* (2014), Dec., pp. 303-308
[6] Lucian, M., *et al*., Impact of Hydrothermal Carbonization Conditions on the Formation of Hydrochars and Secondary Chars from the Organic Fraction of Municipal Solid Waste, *Fuel, 233* (2018), Dec., pp. 257-268
[7] Mukherjee, A., *et al*., Review of Post-Combustion Carbon Dioxide Capture Technologies Using Activated Carbon, *Journal of Environmental Sciences, 83* (2019), Sept., pp. 46-63

[8] Dodevski, V., *et al*., Plane Tree Seed Biomass Used for Preparation of Activated Carbons (Ac) Derived from Pyrolysis, Modeling the Activation Process, *Colloids and Surfaces A: Physicochemical and Engineering Aspects, 522* (2017), June, pp. 83-96
[9] Serna-Guerrero, R., *et al*., Modeling Adsorption of $CO_2$ on Amine-Functionalized Mesoporous Silica, 2. Kinetics and Breakthrough Curves, *Chemical Engineering Journal, 161* (2010), 1-2, pp. 182-190
[10] de Menezes, E. W., *et al*., Ionic Silica Based Hybrid Material Containing the Pyridinium Group Used as an Adsorbent for Textile Dye, *Journal of Colloid and Interface Science, 378* (2012), 1, pp. 10-20
[11] Hancock, J. D., *et al*., Method of Comparing Solid-State Kinetic Data and its Application to the Decomposition of Kaolinite, Brucite and $BaCO_3$, *Journal of the American Ceramic Society, 55* (1972), 1, pp. 74-77
[12] Meng, H., *et al*., Thermal Behavior and the Evolution of Char Structure During Co-Pyrolysis of Platanus Wood Blends with Different Rank Coals from Northern China, *Fuel, 158* (2015), Oct., pp. 602-611
[13] Bendahou, A., *et al*., Isolation and Structural Characterization of Hemicelluloses from Palm of Phoenix Dactylifera L., *Carbohydrate Polymers, 68* (2007), 3, pp. 601-608
[14] Strezov, V., System Approach to Biomass Pyrolysis: Product Characterization, Bionature 2012, *Proceedings*, 3rd International Conference on Bioenvironment, Biodiversity and Renewable Energies (Eds. P. Din, P. Lorenz), IARIA Conference, St. Maarten, The Netherlands, 2012, pp. 7-11
[15] Vhathvarothai, N., *et al*., An Investigation of Thermal Behaviour of Biomass and Coal During Copyrolysis Using Thermogravimetric Analysis, *International Journal of Energy Research, 38* (2014), 9, pp. 1145-1154
[16] Rowell, R. M., Cell Wall Chemistry, in: *Handbook of Wood Chemistry and Wood Composites*, 2nd Edition, (Ed. R. M. Rowell), CRC Press, Taylor & Francis Group, Boca Raton, Fla., USA, 2013, pp. 33-75
[17] Šestàk, J., *et al*., Study of the Kinetics of the Mechanism of Solid-State Reactions at Increasing Temperatures, *Thermochimica Acta, 3* (1971), 1, pp. 1-12
[18] Davis, R. J., Reaction Engineering Concepts for the Catalytic Conversion of Biorenewable Molecules, in: *Catalysis for the Conversion of Biomass and Its Derivatives*, (Eds. M. Behrens, A.K. Datye), Max Planck Research Library for the History and Development of Knowledge, Proceed. 2, Berlin, 2013, pp. 255-293
[19] Benedict, J. B., *et al*., Kinetics of the Single-Crystal to Single-Crystal Two-Photon Photodimerization of Alpha-Trans-Cinnamic Acid to Alpha-Truxillic Acid, *The Journal of Physical Chemistry A, 113* (2009), 13, pp. 3116-3120
[20] Sadana, A., *Engineering Biosensors – Kinetics and Design Applications*, Academic Press, New York, USA, 2002
[21] Hajjaji, M., *et al*., Chemical and Mineralogical Characterization of a Clay Taken from the Moroccan Meseta and a Study of the Interaction Between its Fine Fraction and Methylene Blue, *Applied Clay Science, 20* (2001), 1-2, pp. 1-12
[22] Thomas, W. J., *Adsorption Technology and Design*, Reed Educational and Professional Publishing, Oxford, UK, 1998
[23] Cordoba-Torres, P., *et al*., Fractional Reaction Order Kinetics in Electrochemical Systems Involving Single-Reactant, Bimolecular Desorption Reactions, *Journal of Electroanalytical Chemistry, 560* (2003), 1, pp 25-33
[24] Shahkarami, S., *et al*., Breakthrough $CO_2$ Adsorption in Bio-Based Activated Carbons, *Journal of Environmental Sciences, 34* (2015), Aug., pp. 68-76
[25] Hahn, M. W., *et al*., Mechanism and Kinetics of $CO_2$ Adsorption on Surface Bonded Amines, *The Journal of Physical Chemistry C, 119* (2015), 8, pp. 4126-4135
[26] Contescu, C. I., *et al*., Activated Carbons Derived from High-Temperature Pyrolysis Og Lignocellulosic Biomass, *C - Journal of Carbon Research, 4* (2018), 3, pp. 51-66
[27] Cha, J. S., *et al*., Production and Utilization of Biochar: A Review, *Journal of Industrial and Engineering Chemistry, 40* (2016), Aug., pp. 1-15

Paper submitted: September 13, 2019
Paper revised: November 11, 2019
Paper accepted: December 29, 2019